FLOW CONDITIONING DESIGN IN THICK LIQUID PROTECTION

S.G. Durbin†, M. Yoda, and S.I. Abdel-Khalik

G. Woodruff School of Mechanical Engineering
Georgia Institute of Technology
Atlanta, GA 30332-0405 USA
†(404) 385-1891 gte397r@mail.gatech.edu

The HYLIFE-II conceptual design proposed using arrays of high-speed oscillating and stationary slab jets, or turbulent liquid sheets, to protect the reactor chamber first walls from damaging neutrons, ions and X-rays. Flow conditioning can be used to reduce turbulent fluctuations in these liquid sheets and thereby reduce surface ripple, or free-surface fluctuations, and delay jet breakup. Several flow conditioning configurations are studied experimentally for vertical turbulent sheets of water issuing downwards from nozzles of thickness (small dimension) δ = 1 cm into ambient air for Reynolds numbers Re = 5.0 × 10^4 and 1.2 × 10^5. In particular, the role of one or more fine screens in the flow conditioner was studied. As the flow conditioning element immediately upstream of the nozzle inlet, fine screens have been shown to have a major impact upon the sheet free-surface geometry. Planar laser-induced fluorescence was used to measure the free-surface geometry of the liquid sheet and its fluctuations in the near field at streamwise distances downstream of the nozzle exit $x \leq 25\delta$. Laser-Doppler velocimetry was used to quantify the impact of different conditioning configurations on the cross-stream velocity component and its fluctuations just upstream of the nozzle exit. The results indicate that minor differences in velocity and velocity fluctuations near the nozzle exit can lead to major variations in free-surface geometry, and that free-surface fluctuations are strongly affected by changes in flow conditioner design, even in the near-field region of the flow. A single-screen configuration was shown to produce the smoothest jets at both Reynolds numbers, with fluctuations of 3.3% at Re = 1.2 × 10^5 and x = 25δ.

I. INTRODUCTION

Thick liquid protection has been suggested as a solution for first wall protection and heat removal in inertial fusion energy (IFE) reactor chambers. The High-Yield Lithium-Injection Fusion Energy (HYLIFE-II) conceptual IFE power plant proposed using liquid sheets, or slab jets, of molten Flibe (Li_2BeF_4) for cooling and attenuation of damaging radiation and target debris.[1] The side walls of the chamber are shielded by a lattice of stationary jets that allows target injection and heavy-ion driver beam propagation, while protecting the reactor chamber first walls from the fusion event. Thick liquid protection can therefore help make fusion energy commercially attractive by reducing chamber size and extending chamber lifetime, thus considerably reducing the cost of electricity produced by fusion.[2]

Nozzle and flow conditioner designs that create smooth stationary jets are important for effective protection of the first walls and final focus magnets. Minimizing the surface ripple, or free-surface fluctuations, of liquid sheets will minimize driver beam clipping while maximizing protection. For effective thick liquid protection, the distance between the driver beam and the jet free surface should not exceed 0.5 cm, or about 0.07δ.[3]

Although previous work has addressed how nozzle geometry affects free-surface smoothness in such flows,[4,5] we are unaware of any work evaluating how different flow conditioner designs affect free-surface smoothness. In channel flows, placing a fine screen (FS) after a honeycomb (HC) section can greatly reduce turbulent fluctuations.[6] Subsequent work shows that adding both a coarse screen upstream of the HC and a second FS downstream of the HC-FS combination is even more effective in reducing such fluctuations.[7]

Experiments were performed for turbulent sheets of water issuing vertically downwards into ambient air at Reynolds numbers $Re = U_o \delta / \nu = 5\times10^4$ and 1.2×10^5, where U_o and δ are the average velocity and the short dimension of the sheet, respectively, at the nozzle exit and ν is the liquid kinematic viscosity. The flows proposed for HYLIFE-II have δ = 7 cm and $Re = 2.4\times10^5$. These results are therefore at about half the prototypical *Re* and a much smaller δ. The effects of three different flow conditioner configurations were evaluated in terms of velocity profiles just upstream of and free-surface smoothness up to 25δ downstream of the nozzle exit.

II. EXPERIMENTAL DESCRIPTION

II. A. Flow Loop

Water, pumped from the bottom receiving tanks, passed through the flow conditioning section and nozzle, forming the liquid sheet in the open test section in the recirculating facility.[8] A chiller was used to keep the water in the receiving tanks 5.5 m below the test section at 24°C. The coordinate system used here has an origin at the center of the nozzle exit, with x along the flow direction and y and z along the long and short dimensions of the nozzle, respectively.

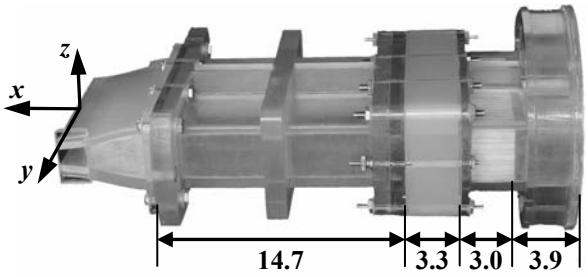

Fig. 1. Flow conditioner assembly (2-S configuration) with LDV nozzle. All dimensions in cm.

The flow conditioner (Fig. 1) in all cases consisted of a stainless steel (SS) perforated plate (50% open area ratio, 4.8 mm diameter staggered holes), PP, followed by a 2.5 cm section of polycarbonate (circular cells of diameter 0.32 cm), HC. The edge-to-edge x-distance between the PP and HC was 3.9 cm. The three different flow conditioner configurations used here were:

1) No screen (0-S): the flow conditioner described above with an edge-to-edge x-distance between the HC and the upstream end of the nozzle of 15.2 cm.
2) One screen (1-S): a SS FS (30 × 30 mesh size, 37.1% open area ratio, 0.33 mm wire diameter, 0.51 mm open cell width), FS-1, was placed 0.5 cm downstream of the downstream end of the HC. This configuration is the same as used in previous studies.[4,5,8]
3) Two screens (2-S): a second SS FS (40 × 40 mesh size, 36.0% open area ratio, 0.25 mm wire diameter, 0.38 mm open cell width), FS-2, was added to the 1-S configuration 3.3 cm downstream of FS-1 using an additional flange.

In the 0-S and 1-S configurations, the overall x-dimension of the flow conditioner was 21.6 cm; it was 24.9 cm for the 2-S configuration. The nozzle downstream of the flow conditioner followed a 5th order polynomial contraction along z with a contraction ratio of 3 and exit y- and z- dimensions of $\delta = 1$ cm and $W_o = 10$ cm, respectively. The nozzle exit had a slight taper with a slope of 4°.[8] One of the two flat sides of the nozzle (fabricated from Vantico 7510 using stereolithography rapid prototyping) was milled away for $-3.6 \text{ cm} \le x \le 0$ and replaced with a 0.56 cm thick flat plate of polycarbonate (Lexan) to provide optical access for LDV measurements.

II. B. Laser-Doppler Velocimetry (LDV)

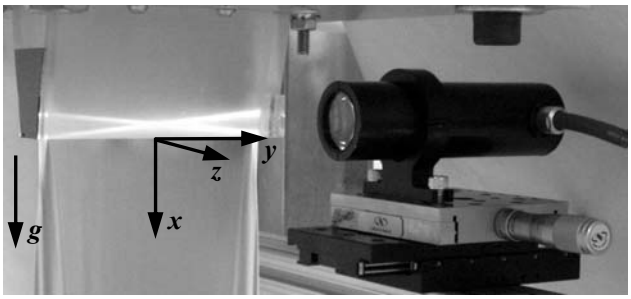

Fig. 2. Photo of LDV probe head and nozzle with optical window (shown obtaining u data).

Velocity and turbulence intensity profiles were measured directly at the nozzle exit using a single-component LDV system (VioSense MiniLDV-80) in backscatter mode with a working distance of 80 mm and a probe volume with FWHM dimensions of 100 × 1200 × 40 μm ($x \times y \times z$) (Fig. 2). Velocity profiles along z were measured at $x = -6$ mm through the polycarbonate window on the flat side of the nozzle. The water in the flow loop was seeded with TiO_2 particles (typical diameter ≈ 0.3 μm) at a volume fraction of about 3.4 ppm.

The Doppler bursts were converted to voltage signals by an avalanche photo-diode (APD), bandpass filtered by a Krohn-Hite 3940, digitized by a National Instruments 5112 onto a PC HD, and converted to velocity using a FFT. The resultant velocity samples were then used to calculate mean and rms fluctuations of the x and z velocity components. Profiles of the mean and rms fluctuations of the x-velocity component u and u', respectively, were obtained at $2.438 \le y/\delta \le 4.838$ with no frequency shift. The probe head was then rotated 90° about y and used to obtain the mean and rms fluctuations of the z-velocity component, or w and w', respectively, with a frequency shift of 1.3 MHz at $1.188 \le y/\delta \le 4.838$. The frequency shift was required to shift the velocity data ($|w| < 1$ m/s) above the pedestal frequency and to resolve directional ambiguities.[9]

Stray reflections of the laser beams at the polycarbonate-water interface made it impossible to obtain data for $y/\delta > 4.838$. Near the center of the flow at $y/\delta = 1.188$, the beam half-angle of the LDV probe of $\kappa = 7.4°$ also precluded obtaining w measurements near the side walls, restricting $|z/\delta| \le 0.17$. The average sampling rate was 20 Hz; 10^3 velocity samples were used to calculate mean and rms fluctuation values. In all cases,

each velocity dataset was acquired over at least $2\times10^4\,\tau$, where the convective time scale $\tau = \delta / U_o$.

III. RESULTS AND DISCUSSION

III. A. LDV Profiles

Profiles were acquired for the three different flow conditioning configurations at Reynolds numbers Re = 5×10^4 and 1.2×10^5. The local nozzle thickness and contraction angle are b = 10.95 mm and 5.5°, respectively. The mean streamwise velocity profiles indicate the flow is uniform for all Reynolds and flow conditioning configurations. The mean transverse velocity profiles vary linearly with z with $|w/U_o| \le \tan(5.5°)(\delta/b)$. The mean velocity profiles for the 1-S configuration are shown in Figure 3. Although not shown here, similar u and w profiles were obtained for the 0-S and 2-S configurations.

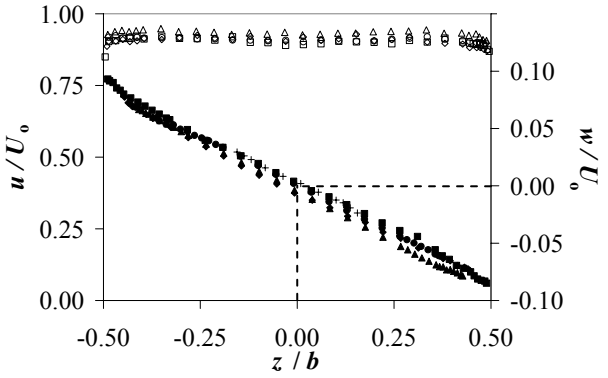

Fig. 3. Normalized profiles of u (open) and w (closed symbols) for 1-S configuration at $Re = 1.2\times10^5$ and y / δ = 4.838 (■), 4.438 (◆), 4.163 (▲), 3.688 (●), and 1.188 (+). Note: Profile at $y / \delta = 1.188$ for w only.

Figure 4 shows normalized profiles of u' and w' for the 1-S configuration at all y-locations. The fluctuations are relatively constant over the central 75% of the flow, or $|z/b| \le 0.375$, with a sharp increase in fluctuations near the nozzle walls due to the turbulent boundary layer. Overall, the streamwise fluctuations are about twice the transverse fluctuations. The 95% confidence level for the u' and w' data is about 0.1%.

Figure 5 compares the velocity fluctuations of the 0-S (◆), 1-S (▲), and 2-S (■) flow conditioning configurations at $Re = 1.2\times10^5$ and $y / \delta = 4.438$. The 2-S configuration exhibits considerably lower u', as compared to 0-S and 1-S. However, measurements of w' do not indicate that the 2-S configuration has lower transverse velocity fluctuations as compared with 1-S.

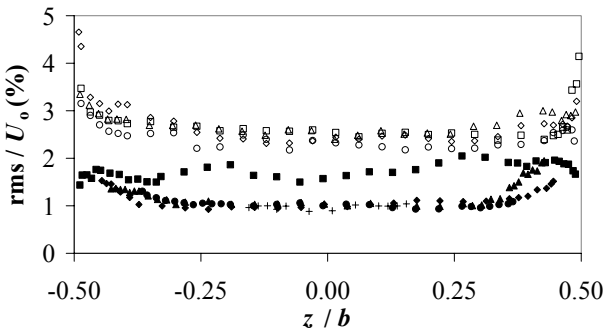

Fig. 4. Normalized profiles of u' (open) and w' (closed symbols) for the 1-S configuration at $Re = 1.2\times10^5$ and y / δ = 4.838 (■), 4.438 (◆), 4.163 (▲), 3.688 (●), and 1.188 (+). Note: Profile at $y / \delta = 1.188$ for w' only.

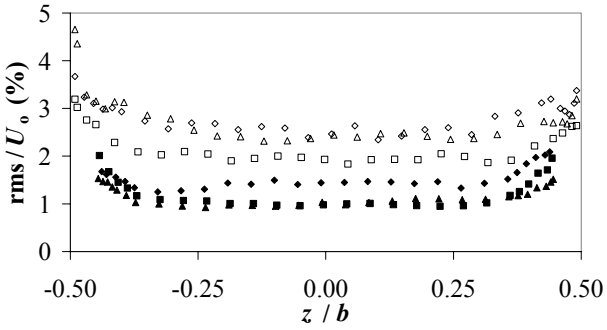

Fig. 5. Normalized profiles of u' (open) and w' (closed symbols) for the 0-S (◆), 1-S (▲), and 2-S (■) flow conditioning configurations at $Re = 1.2\times10^5$ and y / δ = 4.438.

TABLE I. Average Streamwise and Transverse Velocity Fluctuations for $Re = 1.2\times10^5$

	u' / U_o (%)			w' / U_o (%)		
y / δ	0-S	1-S	2-S	0-S	1-S	2-S
4.838	2.6	2.6	2.0	1.7	1.7	1.9
4.438	2.6	2.5	2.0	1.4	1.0	1.0
3.688	2.6	2.3	1.8	1.3	1.1	1.0
1.188	–	–	–	1.9	1.0	1.0
average	2.6	2.5	1.9	1.5	1.2	1.2

Table I summarizes the average velocity fluctuations for characteristic y-locations and all flow conditioning configurations at $Re = 1.2\times10^5$. These results are averaged over $|z/b| \le 0.375$, or the central 75% of the flow. The addition of the second screen reduced the streamwise fluctuations at all locations. The streamwise fluctuations are identical within experimental error for the 0-S and 1-S configurations. Results at $Re = 5\times10^4$ averaged over $|z/b| \le 0.375$ and all y-locations give u' / U_o = 3.1, 2.6, and 2.4% for the 0-S, 1-S, and 2-S configurations, respectively. Although these normalized values are

higher than those for $Re = 1.2\times10^5$, the absolute values of u' are lower.

The measured transverse fluctuations for the 1-S and 2-S configurations are identical within the 95% confidence interval at all locations, although the 0-S case shows marked increases in w' for $y / \delta < 2.438$. Measurements (not included in the table) give normalized values for the 0-S case ranging from 1.6–2.3% for y/δ = 1.638–0.338, respectively. Finally, results at $Re = 5\times10^4$ give spatially averaged values of w' / U_o of 1.8, 1.4, and 1.5% for the 0-S, 1-S, and 2-S configurations, respectively; the absolute values of the transverse fluctuations are again lower than those at $Re = 1.2\times10^5$.

III. B. Free Surface Fluctuations

Planar laser-induced fluorescence (PLIF) was used to obtain the free-surface geometry and calculate the standard deviation of the z-position of the free surface, or σ_z.[8] Technique details are given in Durbin *et. al.*[10] Figure 6 is a graph of σ_z/δ averaged over the central 75% of the flow ($|y/W_o| \le 0.375$) as a function of x/δ for the 1-S (▲) and 2-S (■) configurations at $Re = 5\times10^4$. The 2-S configuration displays higher free surface fluctuations at all downstream locations, even though 1-S and 2-S have nearly identical u' and w'.

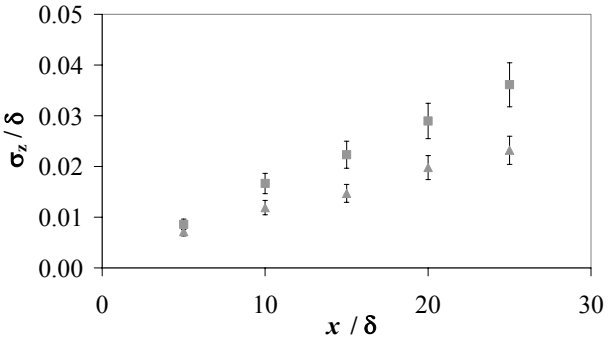

Fig. 6. Graph of σ_z / δ *vs.* x / δ for 1-S (▲) and 2-S (■) flow conditioning configurations at $Re = 5\times10^4$. The error bars denote 95% confidence intervals.

Figure 7 gives the normalized free surface fluctuation as a function of y / δ for 0-S (grey) and 1-S (black symbols). A significant central disturbance is evident in the 0-S case, which was also observed in the transverse velocity fluctuations. The 1-S (and, though not shown here, 2-S) configuration exhibits regions of relatively constant free surface fluctuation near the center of the jet.

Figure 8 compares σ_z/δ as a function of x/δ for the three flow conditioner configurations at $Re = 1.2\times10^5$. The 1-S and 2-S configurations produced jets with similar levels of σ_z. The 0-S configuration yielded significantly rougher jets due in large part to the central disturbance (*cf.* Fig. 7).

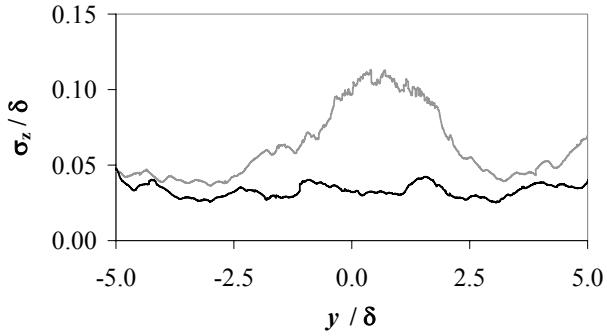

Fig. 7. Plot of σ_z / δ *vs.* y / δ for the 0-S (grey) and 1-S (black) flow conditioning configurations at $x / \delta = 25$ and $Re = 1.2\times10^5$.

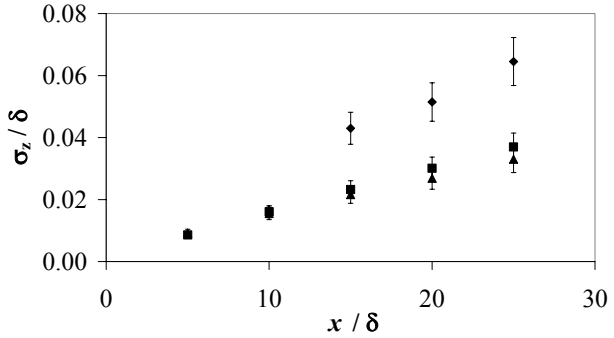

Fig. 8. Plot of σ_z / δ *vs.* x / δ for the 0-S (◆), 1-S (▲) and 2-S (■) flow conditioning configurations at $Re = 1.2\times10^5$. The error bars denote 95% confidence intervals.

III. C. Loss Coefficients

Table II. Loss Coefficient across the Flow Conditioner for $Re = 1.2\times10^5$

Configuration	ΔP (kPa)	U_{in} (m/s)	U_o (m/s)	K_L
0-S	69	2.35	10.72	1.25
1-S	103	2.36	10.75	1.84
2-S	121	2.38	10.84	2.11

The pumping power required to drive the flow scales with the losses across the entire system; here, the flow conditioner / nozzle assembly is a significant source of loss. The impact of adding screens to the flow conditioner was therefore experimentally quantified in terms of the loss coefficient across the flow conditioner / nozzle assembly $K_L = [2(\Delta P) + \rho U_{in}^2]/(\rho U_o^2)$, where ΔP is the pressure loss across the flow conditioner / nozzle, ρ is the fluid density, and U_{in} is the mean velocity at the inlet of the assembly. As expected, adding screens increases ΔP. Table II shows the pressure loss data and

the corresponding loss coefficients at $Re = 1.2\times10^5$ for the three flow conditioning configurations studied here.

IV. CONCLUSIONS

The objective of this study was to quantify the effects of different flow conditioner designs upstream of the nozzle on both velocity fluctuations near the nozzle exit and surface smoothness downstream of the exit. Three conditioner configurations, with zero, one or two screens (denoted by 0-S, 1-S and 2-S, respectively), were evaluated.

At $Re = 1.2\times10^5$, the 0-S configuration had significantly higher transverse velocity rms fluctuations w', and higher σ_z (due to a large central disturbance of the flow) than either the 1-S or 2-S configurations. The 0-S and 1-S configurations had similar levels of streamwise velocity fluctuations u', however. The 2-S configuration had lower u' than either the 0-S or 1-S configurations, as expected from previous studies of flow conditioner designs. But this decrease in streamwise velocity fluctuations was not reflected in surface ripple; the 2-S and 1-S configurations had essentially identical σ_z. Higher levels of streamwise turbulence may actually help stabilize the sheet by increasing the turbulent viscosity. At $Re = 5\times10^4$, similar trends were observed except that the 2-S configuration has higher σ_z than the 1-S configuration despite having similar u' and w'.

In terms of implications for thick liquid protection schemes, both the 1-S and 2-S configurations meet the surface ripple criteria for HYLIFE-II at *Re* up to about half the prototypical value, with $\sigma_z < 0.04\delta$ over the range of downstream distances studied. The 0-S configuration did not meet this criterion with $\sigma_z > 0.06\delta$. Given that the loss coefficient across the flow conditioner for the 2-S configuration is 69% and nearly 15% greater than that for the 0-S and 1-S configurations, respectively, a flow conditioner design with a single screen appears to be the best compromise between surface smoothness and pumping power.

In terms of the fluid dynamics of turbulent liquid sheets, this work has demonstrated that even quite small changes in velocity fluctuations can significantly impact free-surface smoothness, and that such effects can be quantified and correlated using, for example, LDV. The results at the higher *Re* are in agreement with previous studies that suggest that free-surface wave amplitudes are primarily determined by transverse (*vs.* streamwise) velocity fluctuations, and that higher levels of streamwise velocity fluctuations can actually have a stabilizing effect on free-surface smoothness.[11]

ACKNOWLEDGMENTS

This work was sponsored by the Office of Fusion Energy Sciences, US DOE, under award DE-FG02-98ER54499. We thank D.L. Sadowski and T.P. Koehler for their help and support.

REFERENCES

[1] R.W. MOIR, "The High-Yield Lithium-Injection Fusion-Energy (HYLIFE)-II Inertial Fusion Energy (IFE) Power Plant Concept and Implications for IFE," *Phys. Plasmas*, **2**, 2447 (1995).

[2] R.W. MOIR, ET AL, "HYLIFE-II: A Molten-Salt Inertial Fusion Energy Power Plant Design—Final Report," *Fusion Technol.*, **25**, 5 (1994).

[3] J.F. LATKOWSKI and W.R. MEIER, "Heavy-Ion Fusion Final Focus Magnet Shielding Design", *Fusion Technol.*, **39**, 798 (2001).

[4] J.J.R. REPERANT, S.G. DURBIN, M. YODA, S.I. ABDEL-KHALIK and D.L. SADOWSKI, "Studies of turbulent liquid sheets for protecting IFE reactor chamber first walls," *Fusion Eng. Des.*, **63–64**, 627 (2002).

[5] S.G. DURBIN, M. YODA, S.I. ABDEL-KHALIK and D.L. SADOWSKI, "Turbulent Liquid Sheets for Protecting IFE Reactor Chamber First Walls," *Fusion Sci. Technol.*, **44**, 307 (2003).

[6] R.I. LOEHRKE and H.M. NAGIB, "Control of Free Stream Turbulence by Means of Honeycombs: A Balance Between Suppression and Generation," *J. Fluids Eng.*, **98**, 342 (1976).

[7] C. FARELL and S. YOUSSEF, "Experiments on Turbulence Management Using Screens and Honeycombs," *J. Fluids Eng.*, **118**, 26 (1996).

[8] S.G. DURBIN, T.P. KOEHLER, J. REPERANT, M. YODA, S.I. ABDEL-KHALIK and D.L. SADOWSKI, "Surface Fluctuation Analysis for Turbulent Liquid Sheets," *Fusion Sci. Technol.*, **45**, 1 (2004).

[9] F. DURST, A. MELLING and J. WHITELAW, *Principles and Practice of Laser-Doppler Anemometry* (2nd ed.), Academic Press, London (1981).

[10] S.G. DURBIN, M. YODA, and S.I. ABDEL-KHALIK, "Impact of Boundary-Layer Cutting and Flow Conditioning on Free-Surface Behavior in Turbulent Liquid Sheets," *Fusion Sci. Technol.*, To Appear (2005).

[11] K. HEUKELBACH, "Untersuchung zum Einfluss der Düseninnenströmung auf die Stabilität von flächigen Flüssigkeitsstrahlen" [English translation: An Investigation of the Influence of the Flow Inside the Nozzle upon the Stability of Liquid Sheets], Ph.D. Thesis, Technische Universität Darmstadt.